ISSN: 2755-9351

Journal of Alzheimer's Disease & Reports

SCIENTIFIC Research and Community

Research Article

Open Access

Development of Halogenated Indole-Based Chalcones as New Class of MAO-Inhibitors

Jayalakshmy Bahuleyan[1], Stephanus J Cloete[2], Muzammil Kabier[1], Sachithra Thazhathuveedu Sudevan[1], Sunil Kumar[1], Harish Chandra Vishwakarma[1], Della Grace Thomas Parambi[2], Naseer Maliyakkal[4], Anél Petzer[2], Jacobus P Petzer[2]*, Subin Mary Zachariah[1]* and Bijo Mathew[1]*

[1]Department of Pharmaceutical Chemistry, Amrita School of Pharmacy, Amrita Vishwa Vidyapeetham, AIMS Health Sciences Campus, Kochi 682 041, India

[2]Centre of Excellence for Pharmaceutical Sciences, North-West University, Potchefstroom 2520, South Africa

[3]Department of Pharmaceutical Chemistry, College of Pharmacy, Jouf University, Sakaka, Aljouf 72341, Saudi Arabia

[4]Department of Basic Medical Sciences, College of Applied Medical Sciences, Khamis Mushait, King Khalid University, 62569, Kingdom of Saudi Arabia

ABSTRACT

The design and synthesis of chalcones based on halogenated indole are the main topics of this investigation. Ten derivatives were synthesized by introducing halogen substitutions (F, Cl, Br) at the aromatic B ring's ortho, meta, and para positions. (**I-1 to I-10**). These compounds' in vitro inhibitory activity towards monoamine oxidases was subsequently determined. Among them, compound **I-2** exhibited potent MAO-A inhibition with an IC50 of 0.823±0.045 μM, while compound I-4, with an IC50 of 0.014 ±0.008 μ, showed excellent MAO-B inhibition implying that MAO-B selectivity is improved by parachloro substitution. To assess Central Nervous System (CNS) drug-likeness, the lead molecules were subjected to PAMPA method. The results showed that compound **I-2** displayed significant CNS permeability with a Pe value exceeding 4.0×10^{-6} cm/s. Molecular docking revealed that compounds **I-2** and **I-4** exhibited unique binding interactions compared with the reference drug safinamide, including π-π stacking with TYR-398 and hydrogen bonding with CYS-171, while retaining a conserved hydrogen bond with GLN-206. In silico pharmacokinetic studies further indicated that **I-2** and **I-4** possess favorable properties, including effective Blood-Brain Barrier (BBB) penetration. Considering these findings, halogenated indole-based chalcones, particularly compounds **I-2** and **I-4**, present themselves as noteworthy lead candidates for addressing neurodegenerative diseases.

***Corresponding author**

Bijo Mathew, Department of Pharmaceutical Chemistry, Amrita School of Pharmacy, Amrita Vishwa Vidyapeetham, AIMS Health Sciences Campus, Kochi 682 041, India.

Subin Mary Zachariah, Department of Pharmaceutical Chemistry, Amrita School of Pharmacy, Amrita Vishwa Vidyapeetham, AIMS Health Sciences Campus, Kochi 682 041, India.

Jacobus P Petzer, Centre of Excellence for Pharmaceutical Sciences, North-West University, Potchefstroom 2520, South Africa.

Received: September 26, 2025; **Accepted:** October 08, 2025; **Published:** October 20, 2025

Keywords: Indole, Chalcones, Halogen Substitution, Monoamine Oxidase Inhibitors, Neurodegenerative Diseases, Blood-Brain Barrier Permeability, Pampa Assay, Molecular Docking

Introduction

A class of clinical illnesses known as Neurodegenerative Disorders (NDDs) is defined by the progressive, irreversible degeneration and loss of function of neurons in the central and peripheral nervous systems. Aging and age-related comorbidities are considered the major risk factors for the onset and progression of these conditions [1-2]. Many NDDs share overlapping pathogenic mechanisms, despite having different clinical presentations. These mechanisms include oxidative stress and excessive production of Reactive Oxygen Species (ROS); aberrant protein dynamics, such as misfolding, proteasomal dysfunction, defective degradation, and aggregation; DNA damage and impaired mitochondrial bioenergetics; fragmentation of the neuronal Golgi apparatus; disruption of cellular and axonal transport; abnormalities in neurotrophin signaling pathways; and persistent neuroinflammatory or neuroimmune responses. These interrelated processes create vicious loops that eventually lead to neuronal death and the neuron's functional degeneration. Parkinson's Disease (PD) and Alzheimer's Disease (AD) are two prominent instances of these conditions [3-5].

Monoamine Oxidases (MAOs), Flavin-containing enzymes located on the outer mitochondrial membrane, have been implicated in the pathophysiology of NDDs. Through a process dependent on Flavin Adenine Dinucleotide (FAD), two isoforms of MAO-A and MAO-B catalyze the oxidative deamination of biogenic amines, hence modulating neurotransmitter homeostasis [6]. This reaction oxidizes a wide range of primary, secondary, and tertiary amines to their corresponding imines, accompanied by the transfer of two hydrogen atoms to the covalently bound FAD. The imine intermediate naturally hydrolyzes to produce an aldehyde and ammonia, while the reduced flavin is subsequently reacted with by

molecular oxygen to produce hydrogen peroxide (H2O2). Although crucial for normal neurotransmitters metabolism, this process also leads to ROS production, thereby contributing to oxidative stress and neuronal damage that underlie the pathogenesis of AD, PD and other NDDs [7-9]. Clinical evidence highlights the therapeutic importance of targeting these enzymes. Dopamine and serotonin are preferentially metabolized by MAO-A in the Central Nervous System (CNS), with selective MAO-A inhibitors such as clorgyline and moclobemide approved by the FDA for the treatment of depression and anxiety. In contrast, MAO-B metabolizes dopamine and phenylethylamine in the CNS and has emerged as a key therapeutic target in neurodegenerative conditions [10-14]. Clinical use of selective and irreversible MAO-B inhibitors, such as rasagiline and selegiline, as adjuncts or alternatives for L-DOPA in the management of PD also highlights the dual function of MAO inhibition in offering both symptomatic reliefs along with neuroprotection. [15-21].

Indole is a naturally occurring aromatic frame work comprised of up of a benzene ring fused with pyrrole ring. It has steric and electronic characteristics that help it attain pharmacophore and bioavailability as it can interact with various receptors and trigger a variety of biological activities. It thus serves as one of the most efficient frameworks in medicinal chemistry [22]. The indole nucleus seems to be a promising place to start for the design and synthesis of novel derivatives that may protect the Nervous System (NS) against oxidative stress in a variety of chronic and acute neurologic conditions [23]. Numerous indole-based compounds have been investigated in recent literature as effective anti-Alzheimer's and anti-neuroinflammatory agents against both AChE and BuChE in micromolar and nanomolar concentrations [24-27]. The nucleophilic nature of the indole scaffold demonstrated synergistic improvement through bond formation with essential amino acid sequences of enzymes and better bonding of any electronegative group directly attached to it. Additionally, indole has a balanced lipophilic profile which permits the drug to cross the Blood-Brain Barrier (BBB) and strengthens its therapeutics effects. Furthermore, indole had good pharmacokinetic and in vitro metabolic properties, indicating that the whole nucleus is a potentially safe medication [28-31]. The treatment of AD had a major effect by heterocyclic linkers that were attached to indoles [32–34]. As a basic structural scaffold for synthetic and semisynthetic medications, such as pindolol (antihypertensive), oxypertine (antipsychotic), sumatriptan (antimigraine), delavirdine (antiviral), indomethacin (NSAID), Panobinostat (antileukemia), ergotamine (vasoconstrictor), zafirlukast (antiasthmatic), and ondansetron (antiemetic), the indole core is essential to medicinal chemistry [35]. Figure 1:

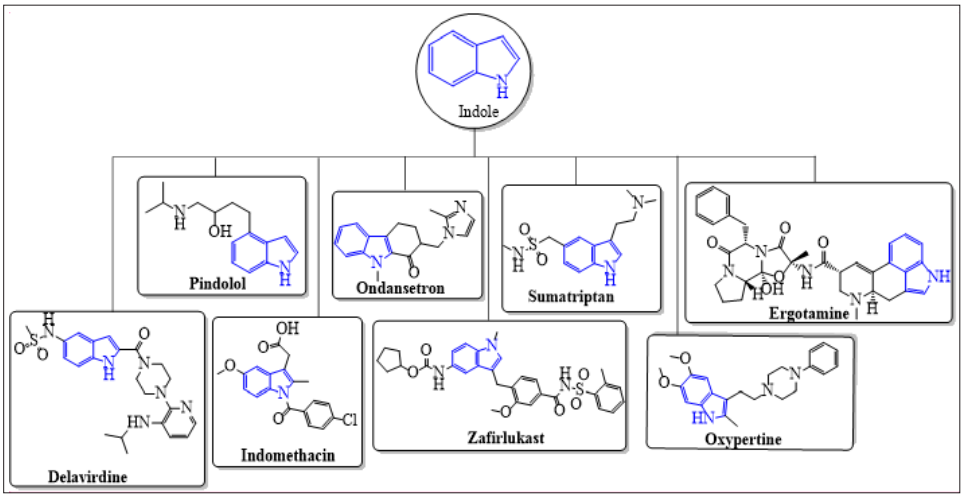

Figure 1: Some FDA-Approved Drugs with Indole Nucleus

Halogens have emerged as key contributors in supramolecular chemistry, with extensive applications in medicinal chemistry [36]. Their electron-withdrawing properties facilitate non-covalent hydrophobic interactions with various enzyme targets, enhancing binding affinity. Recent findings have shown that incorporative halogens into different classes of MAO inhibitors significantly improves MAO-B selectivity. Halogen bonding's stabilizing effect within the enzyme's Inhibitor-Binding Cavity (IBC) is accountable for this enhancement [37]. Based on these findings, the current investigation seeks to develop and discuss chalcones based on halogenated indole and assess the inhibitory profiles of MAO-A and MAO-B [38].

In recent years, chalcones (1,3-diphenyl-2-propen-1-one) and their heteroaryl derivatives have emerged as attractive scaffold in drug discovery (Figure 2) [39-40]. Their α, β-unsaturated carbonyl framework allows structural modifications that enhance bioactivity, with heterocyclic substitutions-particularly indole-based chalcones- exhibiting profound, reversible, and selective inhibition of MAO-B. Beyond MAO inhibition, indole derivatives are well-recognized as privileged structures in medicinal chemistry, owing to their favourable pharmacokinetic properties, Blood-Brain Barrier (BBB) permeability, and wide range of biological activities. Notably, indole-based compounds have shown promising anti-Alzheimer's, anti-neuroinflammatory and neuroprotective effects, making them highly relevant for the treatment of NDDs.

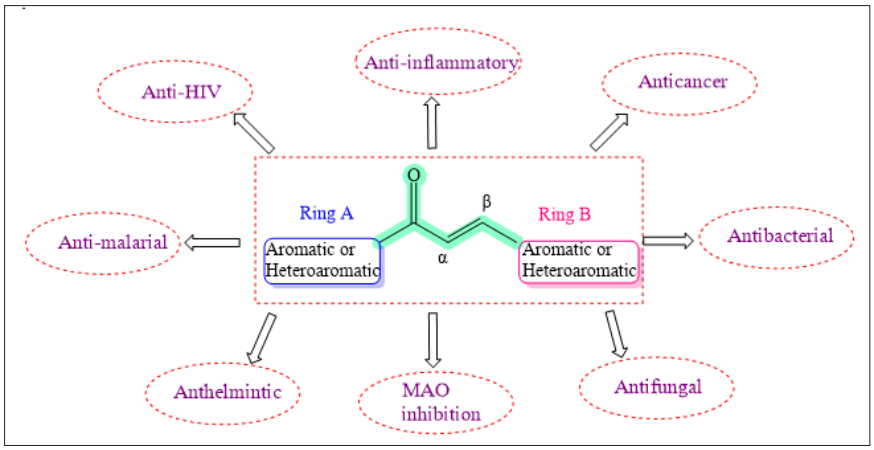

Figure 2: Biological Profile of Heteroaryl Chalcone

Experimental Section

Materials and Methods

All substituted acetophenones and indole-3-carbaldehyde were obtained from Sigma-Aldrich and TCI.A Waters Xevo G2-XS QTOF (Milford, MA, USA) was used for mass spectrometry (MS), while a Bruker Advance Neo 500 MHz NMR spectrometer (Billerica, MA, USA) was used to record 1H and 13C NMR.

Synthesis

Halogenated indole-based chalcone derivatives were synthesized using a conventional synthesis technique. A few drops of piperidine were added as a catalyst after indole-3-carbaldehyde (1 mmol) and the appropriate amount of acetophenone (1 mmol) were dissolved in 20 mL of methanol. The reaction mixture was refluxed for 48 hours at 800–1000 degrees Celsius. After the reaction was completed, the solid product was filtered, washed with methanol, and then recrystallized with ethanol as a solvent. The reaction's progress was monitored using Thin-Layer Chromatography (TLC) with a mobile phase of hexane: ethyl acetate (2:1). These chemicals were further purified by flash column chromatography using hexane: ethyl acetate (100:50) as the mobile phase and silica (mesh size 100–200). Following that, analytical techniques like 1H NMR, 13C NMR, and HRMS were used to structurally confirm these derivatives. The synthetic route is depicted in scheme1

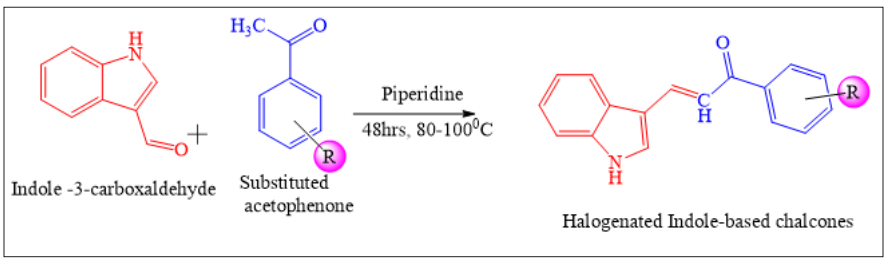

CODE	R	CODE	R
I-1	4-Br	I-6	2-Cl
I-2	3-Br	I-7	4-F
I-3	2-Br	I-8	3-F
I-4	4-Cl	I-9	2-F
I-5	3-Cl	I-10	H

Scheme I: Synthetic Route Adopted for Halogenated Indole- Based Chalcone Derivatives.

MAO Inhibition Studies

Inhibition Profiles

The MAO inhibition potencies were measured corresponding to a published protocol [41,42] using recombinant human MAO-A and MAO-B enzymes (Merck) and kynuramine as the non-selective substrate for both isoforms. Following the completion of the enzyme reactions with sodium hydroxide, fluorescence was identified using spectrometry at an excitation wavelength of 310 nm and emission at 400 nm. Enzyme studies have been performed with and without test inhibitors (range from 0.003 to 100 μM) with the goal to calculate IC50 values. In order to develop sigmoidal curves of catalytic rates against the logarithm of inhibitor concentration (log[I]), enzyme activity data was analyzed and fitted to a one-site competition model in GraphPad Prism 5. These plots were used to calculate the IC50 values, that were then displayed as the mean ± standard deviation of three separate experiments carried out in triplicate.

Kinetic Studies

The MAO inhibition investigations were conducted as previously described, including IC50 value calculation, Lineweaver-Burk graph creation, and time-dependency of inhibition determination [41]. Kynuramine was utilized as the enzyme substrate and commercially available recombinant human MAO-A and MAO-B as the enzyme sources (Merck).

Lineweaver-Burk plots for MAO inhibition were also created using this procedure. The inhibitor concentrations used to determine the MAO catalytic rates were 0.225–0.9 μM for I-2-induced inhibition of MAO-A and 0.0035–0.0175 μM for I-4-induced inhibition of MAO-B. The range of substrate concentrations employed was 15–250 μM. In order to estimate the Ki values, replots of the Lineweaver-Burk plots' slopes against inhibitor concentration were later created.

Reversibility Studies

The MAO enzymes (0.03 mg protein/mL) were preincubated with the test inhibitors for 0, 15, 30, and 60 minutes at room temperature in order to ascertain whether the inhibition was time-dependent. The inhibitors' concentrations were twice as high as their IC50 values. In order to obtain inhibitor concentrations equal to the IC50 value, an enzyme concentration of 0.015 mg protein/mL, and a kynuramine concentration of 50 μM, an equivalent volume of kynuramine was subsequently added to the incubations. Following a further 20 minutes of incubation, the MAO catalytic activities were measured using the previously reported method [42]. The irreversible MAO-A and MAO-B inhibitors, pargyline (13 μM) and (R)-deprenyl (0.04 μM), respectively, were used as controls for the MAO enzymes. The residual MAO activities were then evaluated as previously mentioned.

PAMPA Assay

The parallel artificial membrane permeation assay (PAMPA) is commonly used in early research to evaluate a drug's passive transcellular permeability across the blood-brain barrier. The BBB permeability of lead compounds I-2 and I-4 was assessed using the PAMPA. The supplemental information contains the comprehensive protocol [43].

Computational Studies

ADMET Prediction

The SwissADME web server (http://www.swissadme.ch/index.php) and pKCSM (http://biosig.unimelb.edu.au/pkcsm/) were used to predict the ADMET parameters of the isatin derivatives [44].

Molecular Docking

The RCSB PDB library offered the protein structure for the docking experiment [45]. 2V5Z and 2Z5X are the Human MAO-B and MAO-A complex structures available with co-crystallization of safinamide and harmine respectively [46,47]. MzDOCK was utilized for conducting the molecular docking study [48]. The 10 compound derivatives were prepared with addition of hydrogens at the protonation state of 7.4 pH and energy optimization with MMFF94 [49]. The respective proteins were prepared with addition of hydrogens, adding of missing heavy atoms, gastieger charges, retention of FAD co-factor and removal of other heteroatoms [50]. The protein backbone conformation was validated with Ramachandran plot [51]. Binding site was configured at the site of co-crystal ligand of each protein with a bufferspace of 4 Angstroms. Multiple scoring functions vina, smina, AD4 and vinardo were compared to identify the best scoring function in producing low RMSD poses of co-crystal ligand and to further observe the comparison, a box plot was generated [52-56]. For docking, the selected scoring function was used with exhaustiveness set at 8 and number of modes set at 9. A final redocking was conducted along with the docking of the 10 derivatives and their binding affinity was calculated. The redocked poses were superimposed with the native pose to visualize deviation in the derivation of poses. The 3D interactions of co-crystal ligand and the derivatives were generated and analysed. These led to the conclusion of the study to prove the potential pharmacodynamic property of the compound of interest.

Results and Discussion

Synthesis

Using pyridine as a catalyst, indole-3-carbaldehyde was treated by various substituted acetophenones to create the indole-based chalcone derivatives (I-1–I-10) via a Claisen-Schmidt condensation process (scheme 1). The C-3 carbonyl group of indole-3-carbaldehyde gets more electrophilic in the catalytic medium as the reaction proceeds. This enhanced electrophilicity facilitates the deprotonation of the active methylene group of the ketone, thereby generating a nucleophilic carbanion species. The carbanion subsequently attacks the carbonyl carbon of the indole aldehyde, leading to the formation of an intermediate β-hydroxy ketone. Subsequent dehydration of this intermediate results in the formation of an α, β-unsaturated carbonyl system, which represents the characteristic chalcone framework. Through this process, a new carbon-carbon double bond is formed between the indole nucleus and the acetophenone moiety, yielding the desired indole-based chalcone derivatives in a single step. Spectroscopic methods were used to further analyze and purify the produced chemicals.

The α- and β-protons in the chalcone moiety appeared as doublets in the ^{1}H NMR spectra of I-4 at δ 7.56–7.53 and δ 7.63–7.62, respectively, with a high coupling constant (J = 15 Hz), confirming the double bond's trans configuration. A distinct singlet at δ 8.62 corresponded to the indole NH proton, while the resonances in the aromatic region (δ 7.30–8.10) accounted for the protons of the indole and para-chlorophenyl rings. The ^{13}C NMR spectrum displayed a downfield resonance at δ 189.45, diagnostic of the α, β-unsaturated carbonyl group, together with signals for aromatic carbons between δ 112–139. The HRMS spectrum showed the molecular ion peak at m/z 281.73 $[M+H]^{+}$, consistent with the calculated value of 281.74.

In the case of I-2, the ^{1}H NMR spectrum displayed the β-proton at δ 8.13–8.09 and the α-proton at δ 7.63, again with a significant coupling constant (J ≈ 15 Hz), confirming the trans configuration of the chalcone double bond. The indole NH proton seen as a singlet at δ 8.67, while multiple resonances in the δ 7.40–8.20 region confirmed the aromatic framework of the indole and 3-bromophenyl moieties. The chalcone carbonyl resonance was detected at δ 189.41 in the ^{13}C NMR spectra, while the aromatic carbons were detected between δ 112 and 141. In excellent agreement with the estimated mass of 326.19, the HRMS analysis provided a molecular ion at m/z 326.18 $[M+H]^{+}$.The further details is deposited in the supplementary material

(E)-1-(4-bromophenyl)-3-(1H-indol-3-yl) prop-2-en-1-one(I-1): Orange solid; M. P: 197-198-0C; 1H NMR (500 MHz, DMSO) δ 11.97 (s, 1H, NH),8.13-8.08(m,2H, Ar-H),8.08-8.05(m,3H, Ar-H),7.77-7.75(m,2H, Ar-H),7.63(d,1H, β-CH)7.51-7.50(m,1H, α-CH-)7.27-7.23 (m,2H, Ar-H) 13C NMR (125 MHz, DMSO) δ:189.41, 140.91, 139.72, 137.25, 135.07, 131.36, 130.55, 130.12, 126.84, 125.35, 123.73, 122.90,121.98,120.71,117.30,114.52,112.01. Chemical formula: C17H12BrNO, (HRMS), Calculated 326.19, Observed 326.18

(E)-1-(3-bromophenyl)-3-(1H-indol-3-yl) prop-2-en-1-one(I-2): Orange solid; M.P: 192-1940C; 1H NMR (500 MHz, CDCl3) δ 8.67 (s, 1H, NH),8.17-8.16 (t,1H,Ar-H)8.13-8.09(d,1H,β-CH),8.02-8.00(m,1H,Ar-H),7.97-7.95(d,1H,Ar-H) 7.70-7.63 (m,1H,Ar-H), 7.63 (d,1H,α-CH-), 7.52-7.48(d,1H,Ar-H),7.46-7.44(m,1H,Ar-H)13C-NMR(125MHz,CDCl3) δ:189.41, 140.91, 139.72,137.25,135.07,131.36,130.55,130.12,126.84,125.35,123.73122.90,121.98,120.71,117.30,114.52,112.01.Chemical formula: C17H12BrNO, (HRMS), Calculated 326.19 , Observed 326.18

(E)-1-(2-bromophenyl)-3-(1H-indol-3-yl) prop-2-en-1-one(I-3): Orange solid; 161-1630C; 1H NMR (500 MHz,CDCl3) δ 8.66 (s, 1H, NH),7.70-7.66(m,1H,Ar-H),7.64(d,1H,β-CH-),7.53-7.52(d,1H,α-CH-),7.46-7.45(m,1H,Ar-H),7.43-7.39 (m,2H,Ar-H), 7.33-7.31 (m,1H,Ar-H), 7.30-7.27 (m,2H,Ar-H), 7.17-7.14 (d,1H,Ar-H)13C-NMR(125MHz,CDCl3)δ:195.12, 141.86, 140.99,137.24,133.336,130.90,129.15,127.28,125.23,123.74,122.29,122.02,120.71,119.59,114.21,111.92 Chemical formula: C17H12BrNO, (HRMS), Calculated 326.19 , Observed 326.18.

(E)-1-(4-chlorophenyl)-3-(1H-indol-3-yl) prop-2-en-1-one(I-4): Yellow, solid; M. P: 165-1660C; 1H NMR (500 MHz, CDCl3) δ 8.62 (s, 1H, NH),8.13-8.10 (d,1H,Ar-H),8.02-8.00(m,3H,Ar-H),7.63-7.62(d,1H,β-CH-),7.56-7.53 (d,1H, α-CH-)7.50-7.47 (m, 2H,Ar-H), 7.46-7.45 (m,1H,Ar-H),7.34-7.30(m,2H,Ar-H)13C-NMR(125MHz,CDCl3) δ:189. 45, 139.31, 138.58, 137.34, 137.25, 130.36, 129.77, 128.83, 125.36,123.69,121.92,120.71,117.43,114.56,111.98. Chemical formula: C17H12ClNO, (HRMS), Calculated 281.74, Observed 281.73.

(E)-1-(3-chlorophenyl)-3-(1H-indol-3-yl) prop-2-en-1-one(I-5) : Yellow, solid; M. P: 186-1880C; 1H NMR (500 MHz, CDCl3) δ: 8.64 (s,1H,NH),8.13-8.10(d,1H,Ar-H)8.02-8.00(m,2H,Ar-H)7.93-7.91(m,1H,β-CH-)7.64-7.63 (d,1H , α-CH-),7.55-7.50(m,2H,Ar-H),7.46-7.43(m,2H,Ar-H),7.34-7.32(m,2H,Ar-H). 13C NMR (125MHz, CDCl3) δ:189.46, 140.69, 139.66,137.24,134.81,132.15,130.51,129.86,128.44,126.40,125.35,123.72,121.98,120.72,117.35,114.54,111.99 Chemical formula: C17H12ClNO, (HRMS), Calculated 281.74, Observed 281.73.

(E)-1-(2-chlorophenyl)-3-(1H-indol-3-yl) prop-2-en-1-one (I-6): Yellow, solid; M. P: 150-1520C; 1H NMR (500 MHz, CDCl3) δ 8.88 (s, 1H, NH),7.94-7.93(t,1H, Ar-H),7.73-7.70(d,1H, β-CH-),7.51-7.24(m,8H, Ar-H),7.20-7.17 (d,1H, α-CH-) 13C-NMR (125MHz, CDCl3) δ:194.35,140.92,139.79,137.30,131.24,130.91,130.64,130.23,129.29,126.77,125.23,123.68,122.29,121.97,120.65,114.09,112.00, Molecular formula: C17H12ClNO, (HRMS), Calculated 281.74, Observed 281.73.

(E)-1-(4-fluorophenyl)-3-(1H-indol-3-yl) prop-2-en-1-one (I-7): Yellow, solid; M. P: 166-1680C; 1H NMR (500 MHz, CDCl3) δ: 8.60 (s, 1H, NH),8.12-8.07(m,3H, Ar-H),7.62(d,1H, β-CH-),7.58-7.55(d,1H, α-CH-),7.46-7.44(m,1H, Ar-H)7.34-7.30 (m,2H, Ar-H) ,7.20-7.16 (m,2H,Ar-H)13C NMR (125MHz,CDCl3) δ:189.19,166.35, 164.33,139.00, 137.24,135.29, 130.88,130.81, 130.24,125.37,123.65,121.87,120.70,117.49,115.68.115.51,114.56,111.97 Chemical formula: C17H12FNO, (HRMS), Calculated 265.29, Observed 265.28

(E)-1-(3-fluorophenyl)-3-(1H-indol-3-yl) prop-2-en-1-one (I-8) : Yellow, solid; M. P: 171-1730C; 1H NMR (500 MHz, CDCl3) δ: 8.72(s,1H,NH),8.13-8.10(d,1H,Ar-H)8.02-8.00(m,1H,Ar-H)7.84-7.82(m,1H,Ar-H)7.75-7.72 (m,1H, Ar-H),7.62-7.61(d,1H,β-CH-),7.54-7.51(d,1H,α-CH),7.51-7.43(m,2H,Ar-H),7.39-7.30(m,2H,Ar-H)13C NMR (125MHz,CDCl3) δ:189.51, 163.89, 141.25, 141.20,139.64,137.28, 130.60,130.19,130.13,125.34, 124,123.97, 121.96,120.71,119.29,119.12,117.35,112.02 Chemical formula: C17H12FNO, (HRMS), Calculated 265.29, Observed 265.28.

(E)-1-(2-fluorophenyl)-3-(1H-indol-3-yl) prop-2-en-1-one(I-9): Yellow, solid; M. P: 120-1220C; 1H NMR (500 MHz, CDCl3) δ 8.66(s, 1H, NH),8.04-7.99(m,2H,Ar-H)7.84-7.83(m,1H,β-CH-)7.59(d,1H,α-CH-)7.53-7.51(m,2H,Ar-H),7.49-7.42(m,2H,Ar-H),7.32-7.27(m,2H,Ar-H),7.26-7.17(m,2H,Ar-H).13C NMR (125MHz,CDCl3)δ:189.26(C=O),162.11,160.11, 139.02, 137.25, 133.32,133.25,130.96,127.92,127.81,125.36,124.42,123.63,121.91,121.81,121.75,120.79,116.58,116.39,114.49,111.89.Chemical formula: C17H12FNO, (HRMS), Calculated 265.29, Observed 265.28.

(E)-3-(1H-indol-3-yl)-1-phenylprop-2-en-1-one(I-10): Yellow, solid; M. P: 165-1680C; 1H-NMR(500MHz,CDCl3) δ:8.66(s,1H,NH),8.12-8.09(d,1H,Ar-H)8.06-8.05(m,2H,Ar-H)8.03-8.02 (m,1H,β-CH),7.61-7.56(m,3H,Ar-H),7.53-7.50(m,2H,Ar-H),7.46-7.44(m,1H,α-CH),7.33-7.29 (m,2H,ArH).13C NMR (125MHz,CDCl3) δ:190.96,139.03,138.86, 137.26,132.27, 130.17, 5,125.40,123.58,121.81,120.74,118.03,114.59,111.95,Chemical formula:C17H13N O,(HRMS),Calculated 247.30,Observed 247.29.

Monoamine Oxidase Inhibition Studies

Inhibition Profiles

According to Table 1's MAO inhibitory effectiveness (IC50 values), all these indole-based chalcone derivatives were sub micromolar MAO-A inhibitors, with IC50 values that varied from 0.823 to 0. μM. Sub micromolar potencies for the inhibition of MAO-B were likewise established by compounds **I-2, I-4, I-7**, and **I-8** (Table 1). Considering the inhibition profiles, we represented a structure activity relationships (SARs) Figure 3.

Table 1: IC50 Values for in Vitro Inhibition of Human MAO -A and MAO-B.

Compounds	MAO-A (μM ± SD)[a]	MAO-B (μM±SD)[a]	SI[b]
I-1	42.7 ± 26.0	0.020 ± 0.002	2135
I-2	0.823 ± 0.045	0.012 ± 0.001	69
I-3	10.5 ± 1.07	0.392 ± 0.037	27
I-4	41.0 ± 24.2	0.014 ± 0.0008	2929
I-5	1.12 ± 0.123	0.012 ± 0.001	93
I-6	12.0 ± 1.18	0.391 ± 0.023	31
I-7	2.16 ± 0.358	0.012 ± 0.002	180
I-8	2.43 ± 0.200	0.012 ± 0.008	203
I-9	3.04 ± 0.115	0.047 ± 0.007	65
I-10	3.44 ± 0.215	0.033 ± 0.004	104
Safinamide	-	0.099 ± 0.007	-

[a]Values are given as the mean ± Standard Deviation (SD) of Triplicate Measurements

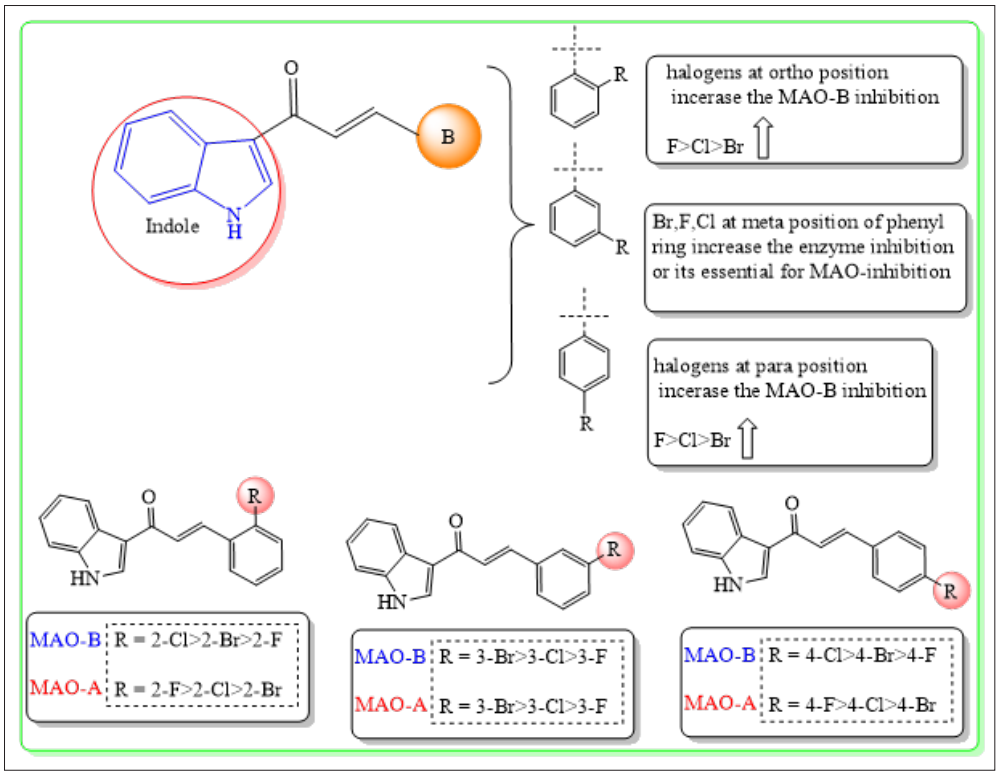

Figure 3: SAR of Halogenated Indole Derivatives

Kinetic Studies

Additionally, Lineweaver-Burk graphs were created for the inhibition of MAO-A and MAO-B by I-2 and I-4, respectively. Figure 4 displays the Lineweaver-Burk graphs for each inhibitor. The graphs were linear and intersected on the y-axis, suggesting that they were indicative of competitive inhibition. I-2 and I-4 were projected to have Ki values of 0.35 and 0.0014 µM, respectively, based on replots of the slopes of the Lineweaver-Burk graphs versus inhibitor concentration (Ki = –y when x = 0).

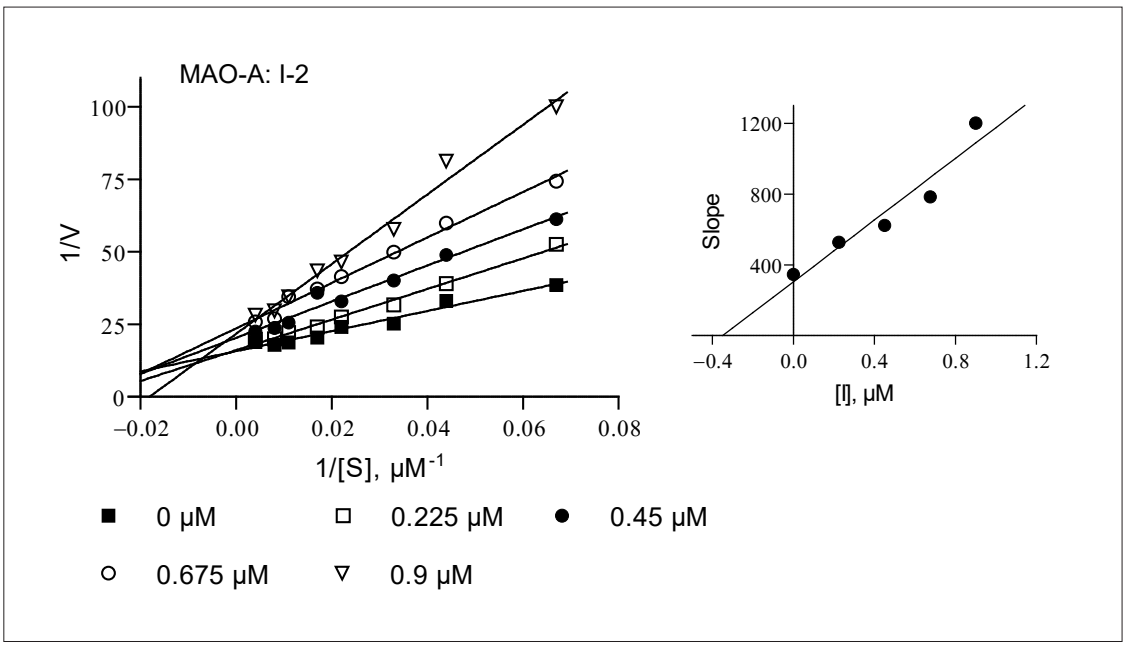

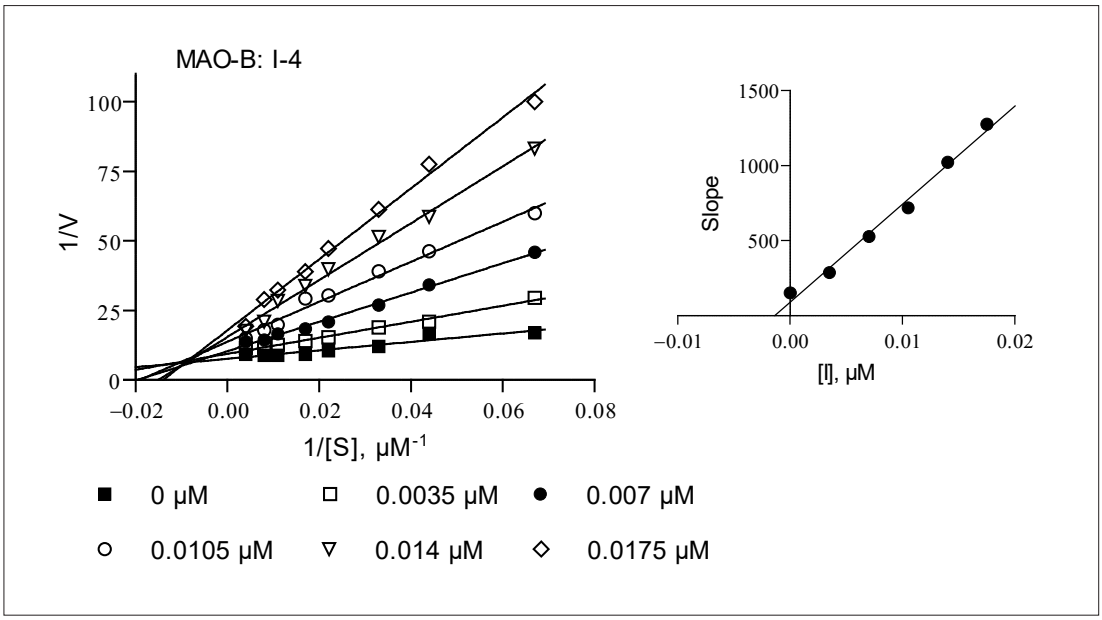

Figure 4: Lineweaver-Burk Plots for the Inhibition of MAO-A and MAO-B. The Insets are Replots for the Slopes of the Lineweaver-Burk Plots Versus Inhibitor Concentration. Ki values of 0.35 and 0.0014 μM were observed for I-2 and I-4, Respectively.

Reversibility Studies

The time-dependency of inhibition was evaluated with the goal to look at the reversibility of MAO inhibition. I-2 and I-4, the study's most powerful MAO-A and MAO-B inhibitors, were chosen for this assessment. The remaining enzyme activity was determined after MAO-A and MAO-B were incubated for 0–60 minutes with I-2 and I-4 present (at a concentration equal to 2 × IC50). The inhibitor concentration was then diluted twofold with the addition of substrate. The findings, which are presented in Figure 5, proved that the degree of inhibition did not rise as the incubation period increased. This suggested that inhibition by I-2 and I-4 was reversible since it was not time-dependent. The longer the enzyme was incubated with the irreversible inhibitors (pargyline and (R)-deprenyl), the lower the enzyme catalytic rates were. This behavior was in consistent with MAO-A and MAO-B being irreversibly inhibited.

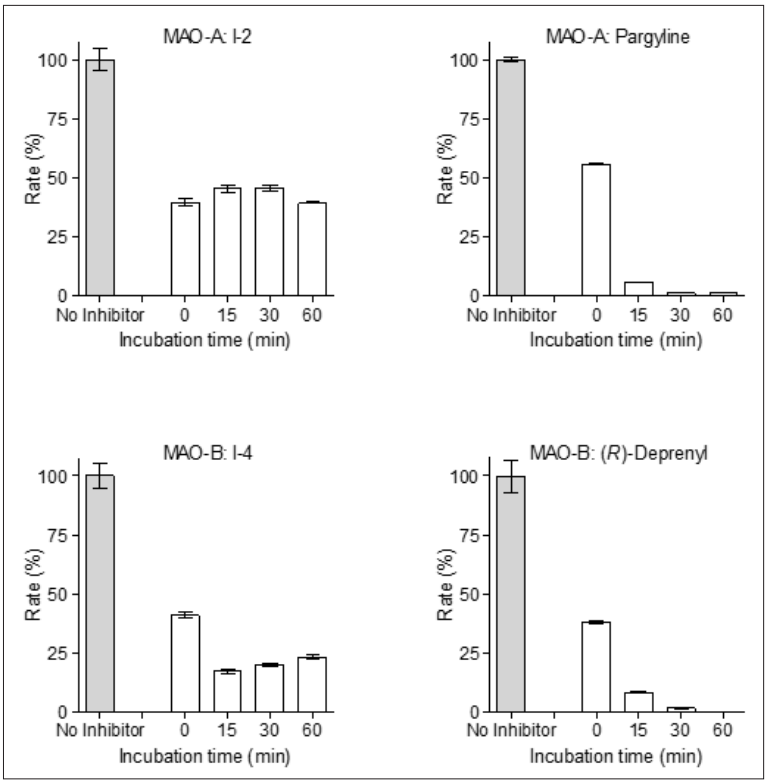

Figure 5: The Time-Dependency of MAO-A and MAO-B Inhibition. the Inhibitors were Preincubated with MAO-A or MAO-B for 0–60 min, and the Residual Enzyme activities were Recorded.

Parallel Artificial Membrane Permeability Assay (PAMPA) for Blood-Brain Barrier (BBB) Permeation Study

With a remarkable high permeability (Pe = 6.57 ± 0.17×10^{-6} cm/s), compound I-2 demonstrated good penetration capacity in the PAMPA testing, indicating its potential for central nervous system bioavailability. This value exceeded that of I-4 (Pe = 4.21 ± 0.11×10^{-6} cm/s) and was the highest recorded. (Table 2).

Drug delivery to the central nervous system (CNS) requires effective brain penetration. The Parallel Artificial Membrane Permeability Assay for the Blood-Brain Barrier (PAMPA-BBB) is used in this study to assess the brain permeability of different derivative compounds. Each compound's effective permeability (Pe) is calculated using known methods to estimate its potential for brain penetration. Compounds with a Pe value greater than 4.0 × 10^{-6} cm/s are categorized as probably brain-permeable (CNS+). A Pe value below 2.0 × 10^{-6} cm/s, on the other hand, indicates a likely failure to cross the blood-brain barrier (CNS-).

Table 2: Blood-Brain Barrier Assay of Key Compounds by Pampa Method.

Compounds	Experimental Pe (×10^{-6} cm·s^{-1})	Prediction
I-2	6.57 ± 0.17	CNS+
I-4	4.21 ± 0.11	CNS+
Selegiline	5.69± 0.04	CNS+

Pe (10^{-6}cm·s^{-1}) > 4.00: CNS+ (high permeation); Pe (10−6cm·s^{-1}) < 2.00: CNS− (low permeation); Pe (10^{-6}cm·s^{-1}) from 2.00 to 4.00: CNS± (BBB permeation uncertain).

Computational Studies

Absorption, Distribution, Metabolism, Excretion and Toxicity (ADMET) Properties

The drug must have adequate intrinsic activity at low therapeutic concentrations, be devoid of harmful side effects, and continue to work until the intended result is obtained. Throughout the drug development process, the ADME (Absorption, Distribution, Metabolism, and Excretion) properties of therapeutic candidates were taken into account in order to optimize pharmacokinetic profiles. In silico pharmacokinetic parameters were calculated using the web-based tool pkCSM (http://biosig.unimelb.edu.au/pkcsm/). The solubility of the compounds in an aqueous environment, expressed as log molar concentration, ranged from -3.92 to -4.98. Given that the small intestine is the primary site for oral drug absorption, the percentage of absorbed pharmaceuticals was quantified. Caco-2 cells, derived from human colon adenocarcinoma, mimic gut epithelial cells, making them a suitable model for predicting oral drug absorption based on Caco-2 permeability. For high permeability, a molecule should exhibit a Papp value exceeding 8 x 10^{-6} cm/s. Notably, all tested molecules demonstrated high permeability, with significant gastrointestinal absorption rates ranging from 91% to 93%. The steady-state volume of distribution (VDss), percentage unbound, and Blood-Brain Barrier (BBB) penetration were used to evaluate the expected drug distribution pattern. When compared to plasma, a log VDss larger than 0.45 indicates a broader drug distribution in tissues. Based on their VDss values, each compound exhibited moderate to weak distribution into tissues. Furthermore, the low blood protein binding of the compounds, as determined by the fraction-bound method, indicates a higher fraction of unbound drug available for pharmacological activity. BBB permeability was evaluated using pkCSM. BBB penetration is crucial for treatments targeting neurodegenerative diseases. While a logBB value of -1 typically suggests weak brain distribution, values greater than 0.3 indicate facile BBB crossing. The compounds' ability to successfully cross the BBB was shown by the logBB values. Compounds with a log PS > -2 are specifically anticipated to penetrate the Central Nervous System (CNS), whereas those with a log PS < -3 are typically regarded as ineffectual. Importantly, CNS permeability was observed for all molecules evaluated in this study. Regarding metabolism, each compound demonstrated specific interactions with cytochromes, acting either as an inhibitor or a substrate. The analysis indicated an overall clearance for all compounds ranging from -0.091 to 0.384 log mL/min/kg. In conclusion, all compounds exhibited favourable ADME characteristics, making them promising candidates [45,46].

Table 3: Synthesized Compounds (I-1 to I-10) for Predicted ADME Properties.

Code	Absorption			Distribution				Metabolism	Excretion Total Clearance (logml/min/kg)
	Log S (log mol/L)	Caco-2 perm. (log Papp in 10^{-6} cm/s)	Int. abs.(% Absorbed)	VDss (log L/kg)	Fract. Unb(Fu)	BBB perm. (log BB)	CNS perm. (log PS)		
I-1	-5.187	1.454	91.545	0.361	0.03	0.285	-1.013	CYP2D6, CYP3A4 substrate CYP1A2, CYP2C19, CYP2C9, CYP2D6, CYP3A4 inhibitor	-0.112

I-2	-5.198	1.573	91.558	0.384	0.025	0.276	-1.031	CYP2D6, CYP3A4 substrate CYP1A2, CYP2C19, CYP2C9, CYP2D6, CYP3A4 inhibitor	0.006
I-3	-5.187	1.628	91.992	0.365	0.025	0.278	-1.031	CYP2D6, CYP3A4 substrate CYP1A2, CYP2C19, CYP2C9, CYP3A4 inhibitor	0.009
I-4	-5.11	1.454	91.612	0.343	0.033	0.033	-1.013	CYP2D6, CYP3A4 substrate CYP1A2, CYP2C19, CYP2C9, CYP3A4 inhibitor	-0.091
I-5	-5.121	1.573	91.625	0.367	0.028	0.277	-1.031	CYP2D6, CYP3A4 substrate CYP1A2, CYP2C19, CYP2C9, CYP2D6, CYP3A4 inhibitor	0.029
I-6	-5.111	1.628	92.059	0.347	0.028	0.28	-1.031	CYP2D6, CYP3A4 substrate CYP1A2, CYP2C19, CYP2C9, CYP2D6, CYP3A4 inhibitor	0.101
I-7	-4.814	1.364	92.651	0.18	0.048	0.279	-1.058	CYP3A4 substrate CYP1A2, CYP2C19, CYP2C9 inhibitor	0.269
I-8	-4.827	1.17	92.636	0.169	0.046	0.274	-1.083	CYP3A4 substrate CYP1A2, CYP2C19, CYP2C9, CYP3A4 inhibitor	0.264
I-9	-4.767	1.588	93.091	0.132	0.045	0.277	-1.088	CYP3A4 substrate CYP1A2, CYP2C19, CYP2C9 inhibitor	0.201

I-10	-4.733	1.606	92.582	0.287	0.041	0.314	0.314	CYP2D6, CYP3A4 substrate CYP1A2, CYP2C19, CYP2C9, CYP2D6 inhibitor	0.384

Note: The pharmacokinetic properties were calculated in silico usingonlinedatabasepkCSM(http://biosig.unimelb.edu.au/pkcsm/). Molecules with Log BB > 0.3 are considered readily to cross the BBB, while molecules with logBB < -1 are poorly distributed to the brain. Compounds with log PS > -2 are considered to penetrate the CNS, while those logPS < -3 are considered unable to penetrate the CNS. perm., permeability.

Molecular Docking

Ramachandran Plot of 2V5Z and 2Z5X

To account for their variances in nature, the ϕ and ψ angles of every amino acid—aside from glycine, proline, and pre-proline—were displayed in a generic figure 6. The plot is shown in Figure 6 for each protein. To ascertain whether the amino acids are located inside the energetically favourable contours, the plot was examined.

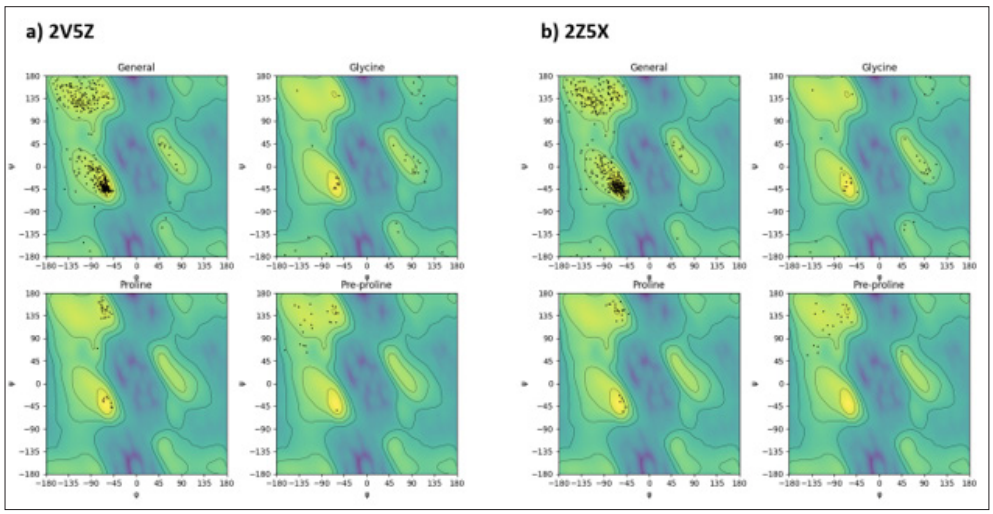

Figure 6: Ramachandran Plot of the Amino Acids Proline, Glycine, Pre-Proline, and General (a) 2V5Z, b) 2Z5X. The Amino Acids Were Found to be within the Angles that were Favourable to Energy.

Comparison of Scoring Function with Iterative Redocking

To remove the impact of random seed in the Iterative Local Search protocol within the Smina docking engine, the six scoring functions that were available in MzDOCK were iteratively redocked five times. The findings are displayed as a box plot in Figure 7, which can be used to determine the most accurate scorer for obtaining high resolution poses.

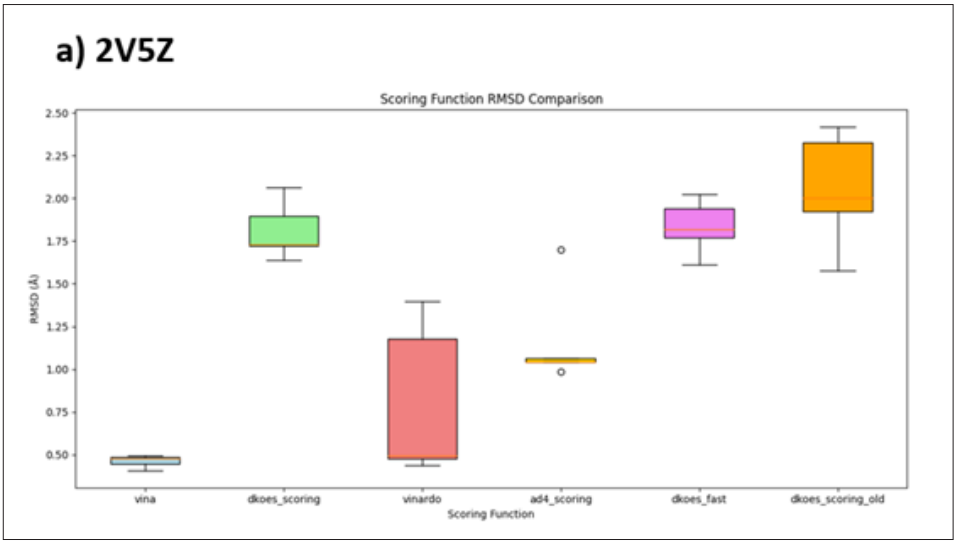

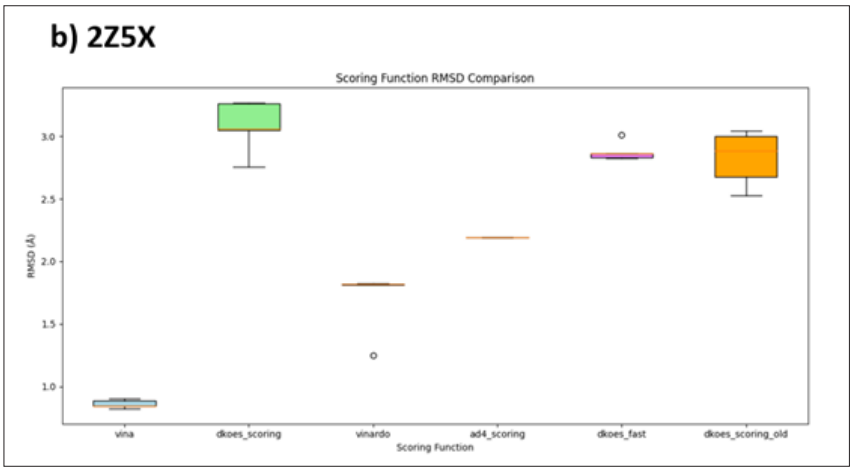

Figure 7: Box Plot with the RMSD between Crystallographic and Redocked Positions for each Scoring Function on the X-axis. In both cases, the Vina Scoring Function was Shown to be the most accurate. a) 2V5Z, b) 2Z5X

Table 3: Redocking RMSD for Each Target

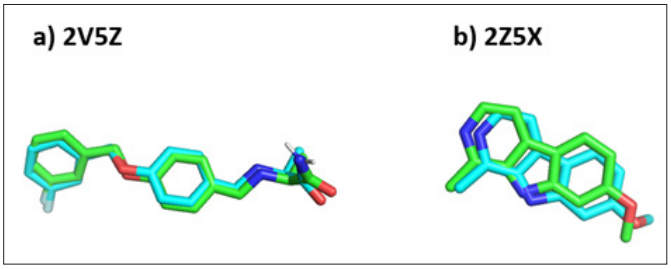

Targets	RMSD(A)
2V5Z	0.424
2Z5X	0.856

Figure 8: The Co-crystal Ligand's Native and Superimposed Redocked Poses within Targets a) 2V5Z and b) 2Z5X. The Ligands with the Colours Green and Cyan Stand for Native and Redocked Posture, Respectively.

Binding Affinity and 3D Interactions

The study's compounds were docked using the Vina scoring function and Table 4 compares each compound's binding affinity for each target to that of its corresponding standard co-crystallized ligand.

Table 4: Binding Affinity of Compounds in MAO-A and MAO-B

Compound ID	Binding Affinity (kcal/mol)	
	MAO-A	MAO-B
I-1	-9.9	-10.7
I-2	-9.1	-10.7
I-3	-8.3	-10.5
I-4	-9.9	-10.7
I-5	-9.3	-10.7
I-6	-8.6	-10.8
I-7	-9.7	-10.6
I-8	-9.5	-10.7
I-9	-9.4	-10.5
I-10	-9.3	-10.4
co-crystal ligand	-8.7	-10.2

From the Table 4, its evident that all the derivatives perform well when compared with the co-crystal ligand for both proteins. Since I-1 and I-4 had the most selective index value, there interactions were compared with co-crystal ligand of both proteins in Figure 9 and Figure 10 respectively.

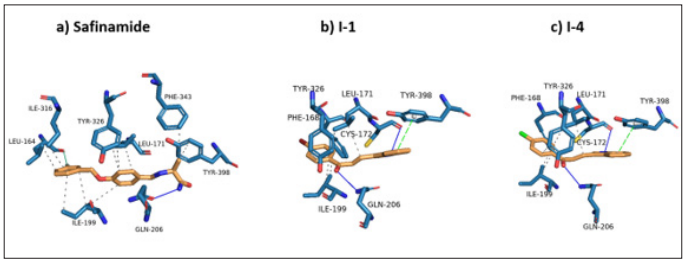

Figure 9: The 3D Interaction of Compounds Rocked at 2V5Z Represented in Orange Colour with Amino Acids Represented in Blue Colour. The Dashed Grey Bond Indicates Hydrophobic Interactions, Blue Coloured Bond Indicates Hydrogen Bonding, Cyan Coloured Bond Represents Halogen Bonding and the Green Dashed Line Represent π-π Stacking

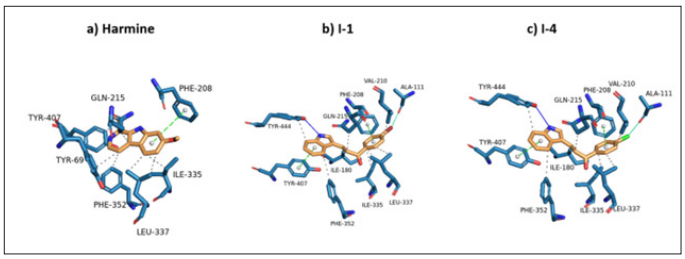

Figure 10: The 3D Interaction of Compounds Docked at 2Z5X represented in Orange Colour with Amino Acids Represented in Blue Colour. The Dashed Grey Bond Indicates Hydrophobic Interactions, Blue Coloured Bond Indicates Hydrogen Bonding, Cyan Coloured Bond Represents Halogen Bonding and the Green Dashed Line represent π-π Stacking.

The Interaction patterns in Figure 10 reveal that I-1 and I-4 forms a new binding profile compared to the safinamide by forming pi-pi bond with TYR-398 and hydrogen bond with CYS-171, although the GLN-206 H-bond was same for the derivatives and the safinamide. Furthermore, some hydrophobic interactions were captured to be similar such as with LEU171, TYR326 and ILE199. This indicates promise to the potential of the compound as it retains certain interaction profile but adds in new binding interactions. This is

crucial since the safinamide binding mode could possibly lead to desolvation penalty due to uncompromised polar atoms, but this is not case in I-1 and I-4. The Interaction patterns in Figure 10 shows that the compounds I-1 and I-4 is in clear complementarity with the interaction profile to harmine, but still there are addition of other interactions like Pi-Pi bond with TYR-407, H-bond with TYR-444 and Halogen bond with ALA-111. The carbonyl group of the compounds not forming h-bond might make it less stable and cause huge desolvation penalty. All the derivatives showed promising binding profile compared to standard co-crystal ligand. Notably, I-1 and I-4 had new binding profile compared to safinamide which are retaining some of its interactions while leading to other favourable interaction leading to better desolvation and anchoring. Although, I-1 and I-4 has great interaction and affinity profile in MAO-A as well. There is reason of scepticism given that the rotatable bonds around the carbonyl group, Absence of a stabilizing hydrogen bond to this moiety could compromise conformational stability in the binding site, potentially leading to reduced binding affinity in practice. Since prospective studies showed that I-1 and I-4 were highly selective to MAO-B, A valid reasoning might be the new binding mode obtained by the compounds favourable in terms of approximate desolvation and anchoring with polar interactions. The compounds could be studied with further experiments to validate its theoretical selectivity.

Conclusion

The successful design and synthesis of halogenated indole-based chalcones as a novel class of monoamine oxidase inhibitors is highlighted in this paper. Parachloro substitution (compound I-4) provided the most powerful and selective MAO-B inhibitory profile, whereas compound I-2 showed substantial MAO-A inhibition. Systematic halogen substitution at various locations of the aromatic B ring altered the biological activity. The lead compounds' potential ability to traverse the blood-brain barrier was further supported by their favorable CNS permeability in PAMPA experiments and encouraging in silico pharmacokinetic predictions. New pathways for selective MAO inhibition were suggested by molecular docking, which also showed unique binding interactions when compared to the reference medication safinamide.

Acknowledgment

The authors extend their appreciation to the Deanship of Research and Graduate Studies at King Khalid University for funding this work through Small Research Project under grant number RGP1/149/46.

References

1. Jellinger KA (2024) Behavioral disorders in Parkinson disease: current view. Journal of Neural Transmission 1-33.
2. Bijo Mathew, Della Grace Thomas Parambi (2024) Enzymes in Neurodegenerative Disorders: Mechanism and Therapeutic Potentials. https://link.springer.com/book/10.1007/978-981-97-6822-6.
3. Jellinge KA (2009) Recent advances in our understanding of neurodegeneration. Journal of neural transmission 116: 1111-1162.
4. Hague (SM) Klaffke S, Bandmann O (2005) Neurodegenerative disorders: Parkinson's disease and Huntington's disease. Journal of Neurology, Neurosurgery & Psychiatry 76: 1058-1063.
5. Erkkinen MG, Kim MO, Geschwind MD (2018) Clinical neurology and epidemiology of the major neurodegenerative diseases. Cold Spring Harbor perspectives in biology 10: 033118.
6. Ramsay R (2012) Monoamine oxidases: the biochemistry of the proteins as targets in medicinal chemistry and drug discovery. Current topics in medicinal chemistry 12: 2189-2209.
7. Youdim MB, Edmondson D, Tipton KF (2006) The therapeutic potential of monoamine oxidase inhibitors. Nature reviews neuroscience 7: 295-309.
8. Jenner P, Olanow CW (1996) Oxidative stress and the pathogenesis of Parkinson's disease. Neurology 47: 161S-170S.
9. Youdim MB, Bakhle YS (2006) Monoamine oxidase: isoforms and inhibitors in Parkinson's disease and depressive illness. British journal of pharmacology 147: S287-S296.
10. Tipton KF (2018) 90 years of monoamine oxidase: some progress and some confusion. Journal of Neural Transmission 125: 1519-1551.
11. Lum CT, Stahl SM (2012) Opportunities for reversible inhibitors of monoamine oxidase-A (RIMAs) in the treatment of depression. CNS spectrums 17: 107-120.
12. Naoi M Maruyama W, Shamoto-Nagai M (2018) Type A monoamine oxidase and serotonin are coordinately involved in depressive disorders: from neurotransmitter imbalance to impaired neurogenesis. Journal of Neural Transmission 125: 53-66.
13. Youdim MB, Edmondson D, Tipton KF (2006) The therapeutic potential of monoamine oxidase inhibitors. Nature reviews neuroscience 7: 295-309.
14. Tripathi RKP, Ayyannan SR (2019) Monoamine oxidase-B inhibitors as potential neurotherapeutic agents: An overview and update. Medicinal research reviews 39: 1603-1706.
15. Guglielmi P, Carradori S, Ammazzalorso A, Secci D (2019) Novel approaches to the discovery of selective human monoamine oxidase-B inhibitors: is there room for improvement?. Expert Opinion on Drug Discovery 14: 995-1035.
16. Carradori S, Silvestri R (2015) New frontiers in selective human MAO-B inhibitors: Miniperspective. Journal of medicinal chemistry 58: 6717-6732.
17. Dezsi L, Vecsei L (2017) Monoamine oxidase B inhibitors in Parkinson's disease. CNS & Neurological Disorders-Drug Targets (Formerly Current Drug Targets-CNS & Neurological Disorders) 16: 425-439.
18. Joy M, Mathew B, Sudarsanakumar C (2018) Structural features of Safinamide: a combined Hirshfeld surface analysis & quantum chemical treatment. Chemical Data Collections 17: 404-414.
19. Bolasco A, Carradori S, Fioravanti R (2010) Focusing on new monoamine oxidase inhibitors. Expert Opinion on Therapeutic Patents 20: 909-939.
20. Krösser S, Marquet A, Gallemann D, Wolna P, Fauchoux N, et al. (2012) Effects of ketoconazole treatment on the pharmacokinetics of safinamide and its plasma metabolites in healthy adult subjects. Biopharmaceutics & drug disposition 33: 550-559.
21. Nasir Abbas Bukhari S, Jantan I, Jasamai M (2013) Anti-inflammatory trends of 1, 3-diphenyl-2-propen-1-one derivatives. Mini reviews in medicinal chemistry 13: 87-94.
22. Kaushik NK, Kaushik N, Attri P, Kumar N, Kim CH, et al. (2013) Biomedical importance of indoles. Molecules 18: 6620-6662.
23. Štolc S (1999) Indole derivatives as neuroprotectants. Life sciences 65: 1943-1950.
24. Taha M, Rahim F, Uddin N, Khan IU, Iqbal N, et al. (2021) Exploring indole-based-thiadiazole derivatives as potent acetylcholinesterase and butyrylcholinesterase enzyme inhibitors. International Journal of Biological Macromolecules 188: 1025-1036.
25. Lamie PF, Abdel-Fattah MM, Philoppes JN (2022) Design and synthesis of new indole drug candidates to treat Alzheimer's disease and targeting neuro-inflammation using a multi-target-directed ligand (MTDL) strategy. Journal of enzyme inhibition and medicinal chemistry 37: 2660-2678.

26. Khan S, Iqbal S, Taha M, Rahim F, Shah M, et al. (2022) Synthesis, in vitro biological evaluation and in silico molecular docking studies of indole based thiadiazole derivatives as dual inhibitor of acetylcholinesterase and butyrylchloinesterase. Molecules 27: 7368.
27. Ferreira JP, Albuquerque HM, Cardoso SM, Silva AM, Silva VL (2021) Dual-target compounds for Alzheimer's disease: natural and synthetic AChE and BACE-1 dual-inhibitors and their structure-activity relationship (SAR). European Journal of Medicinal Chemistry 221: 113492.
28. Azmy EM, Nassar IF, Hagras M, Fawzy IM, Hegazy M, et al. (2023) New indole derivatives as multitarget anti-Alzheimer's agents: synthesis, biological evaluation and molecular dynamics. Future Medicinal Chemistry 15: 473-495.
29. Ahmad M (2020) Donepezil: A review of the recent structural modifications and their impact on anti-Alzheimer activity. Brazilian Journal of Pharmaceutical Sciences 56: 18325.
30. Wang J, Wang ZM, Li XM, Li F, Wu JJ et al. (2016) Synthesis and evaluation of multi-target-directed ligands for the treatment of Alzheimer's disease based on the fusion of donepezil and melatonin. Bioorganic & Medicinal Chemistry 24: 4324-4338.
31. Pudlo M, Luzet V, Ismaïli L, Tomassoli I, Iutzeler A, et al. (2014) Quinolone–benzylpiperidine derivatives as novel acetylcholinesterase inhibitor and antioxidant hybrids for Alzheimer Disease. Bioorganic & medicinal chemistry 22: 2496-2507.
32. Dong-Dong LIU, Zhang FF, Ming GAO, Jun-Chen, ZHOU, et al. (2022) Pt nanoparticle/N-doped graphene nanozymes for colorimetric detection of acetylcholinesterase activity and inhibition. Chinese Journal of Analytical Chemistry 50: 100177.
33. Taha M, Alshamrani FJ, Rahim F, Uddin N, Chigurupati S (2021) Synthesis, characterization, biological evaluation, and kinetic study of indole base sulfonamide derivatives as acetylcholinesterase inhibitors in search of potent anti-Alzheimer agent. Journal of King Saud University-Science 33: 101401.
34. Barril X, Kalko SG, Orozco M, Luque F (2002) Rational design of reversible acetylcholinesterase inhibitors. Mini Reviews in Medicinal Chemistry 2: 27-36.
35. Pravin NJ, Kavalapure RS, Alegaon SG, Gharge S, Ranade SD (2025) Indoles as promising therapeutics: a review of recent drug discovery efforts. Bioorganic Chemistry 154: 108092.
36. Wilcken R, Zimmermann MO, Lange A, Joerger AC, Boeckler FM (2013) Principles and applications of halogen bonding in medicinal chemistry and chemical biology. Journal of medicinal chemistry 56: 1363-1388.
37. Koyiparambath VP, Oh JM, Khames A, Abdelgawad MA, Nair AS, et al. (2021) Trimethoxylated halogenated chalcones as dual inhibitors of MAO-B and BACE-1 for the treatment of neurodegenerative disorders. Pharmaceutics 13: 850.
38. Mathew B, Carradori S, Guglielmi P, Uddin MS, Kim H (2021) New aspects of monoamine oxidase B inhibitors: The key role of halogens to open the golden door. Current Medicinal Chemistry 28: 266-283.
39. Mathew B, Oh JM, Baty RS, Batiha GES, Parambi DGT (2021) Piperazine-substituted chalcones: A new class of MAO-B, AChE, and BACE-1 inhibitors for the treatment of neurological disorders. Environmental Science and Pollution Research 28: 38855-38866.
40. Mathew B, Suresh J, Anbazghagan S, Paulraj J, Krishnan GK (2014) Heteroaryl chalcones: Mini review about their therapeutic voyage. Biomedicine & Preventive Nutrition 4: 451-458.
41. Hussien A, Musa A, El-Din, HTN, Helal AM, et al. (2025) Phenyltriazole-based sulfonamides: novel dual-target agents against MRSA biofilms and resistant pathogens. RSC advances 15: 17186-17202.
42. Mostert S, Petzer A, Petzer JP (2015) Indanones As High-Potency Reversible Inhibitors of Monoamine Oxidase. ChemMedChem 10: 862-873.
43. Di L, Kerns EH, Fan K, McConnell OJ, Carter GT (2003) High throughput artificial membrane permeability assay for blood-brain barrier. Eur. J. Med. Chem 38: 223-232.
44. Pires DEV, Blundell TL, Ascher DB (2015) pkCSM: Predicting small-molecule pharmacokinetic and toxicity properties using graph-based signatures J Med Chem 58: 4066-4072.
45. Mahía SA, Peña-Díaz S, Navarro J, José Galano-Frutos I, Pallarés J Pujols, et al. (2021) Design, synthesis and structure-activity evaluation of novel 2-pyridone-based inhibitors of α-synuclein aggregation with potentially improved BBB permeability, Bioorg Chem 117.
46. Berman HM, Westbrook J, Feng Z, Gilliland G, Bhat TN, et al. (2000) The Protein Data Bank. Nucleic Acids Res 28: 235-242.
47. Binda C, Wang J, Pisani L, Caccia C, Carotti A, et al. (2007) Structures of human monoamine oxidase B complexes with selective noncovalent inhibitors: safinamide and coumarin analogs. J Med Chem 50: 5848-5852.
48. Son SY, Ma J, Kondou Y, Yoshimura M, Yamashita E, et al. (2008) Structure of human monoamine oxidase A at 2.2-A resolution: the control of opening the entry for substrates/inhibitors. Proc Natl Acad Sci USA 105: 5739-5744.
49. Kabier M, Gambacorta N, Trisciuzzi D, Kumar S, Nicolotti O, et al. (2024) MzDOCK: A free ready-to-use GUI-based pipeline for molecular docking simulations. J Comput Chem 45: 1980-1986.
50. Halgren TA (1999) MMFF VII. Characterization of MMFF94, MMFF94s, and other widely available force fields for conformational energies and for intermolecular-interaction energies and geometries. J Comput Chem 20: 730-748.
51. Johann Gasteiger, Mario Marsili (1980) Iterative partial equalization of orbital electronegativity—a rapid access to atomic charges, Tetrahedron 36: 3219-3228.
52. Nnyigide OS, Nnyigide TO, Lee SG, Hyun K (2022) Protein Repair and Analysis Server: A Web Server to Repair PDB Structures, Add Missing Heavy Atoms and Hydrogen Atoms, and Assign Secondary Structures by Amide Interactions. J Chem Inf Model 62: 4232-4246.
53. Eberhardt J, Santos-Martins D, Tillack AF, Forli S (2021) AutoDock Vina 1.2.0: New Docking Methods, Expanded Force Field, and Python Bindings. J Chem Inf Model 61: 3891-3898.
54. Koes DR, Baumgartner MP, Camacho CJ (2013) Lessons learned in empirical scoring with smina from the CSAR 2011 benchmarking exercise. J Chem Inf Model 53: 1893-1904.
55. Morris GM, Huey R, Lindstrom W, Sanner MF, Belew RK, et al. (2009) AutoDock4 and AutoDockTools4: Automated docking with selective receptor flexibility. J Comput Chem 30: 2785-2791.
56. Quiroga R, Villarreal MA (2016) Vinardo: A Scoring Function Based on Autodock Vina Improves Scoring, Docking, and Virtual Screening. PLoS One 11: 0155183.